Title: BDNF signaling in Hebbian and Stentian structural plasticity in the developing visual system

Authors: Elena Kutsarova[1,2], Anne Schohl[1], Martin Munz[1,3,4] Alex Wang[1,5], Yuan Yuan Zhang[1,6], Olesia M Bilash[1,7], Edward S Ruthazer[1]*

Affiliations:1. Montreal Neurological Institute-Hospital, McGill University, Montreal, QC H3A 2B4, Canada

2. Max Planck Institute for Brain Research, 60438 Frankfurt, Germany

3. Central Visual Circuits Group, Institute of Molecular and Clinical Ophthalmology Basel, 4031 Basel, Switzerland

4. Department of Ophthalmology, University of Basel, 4056 Basel, Switzerland

5. Interdepartmental Neuroscience, Yale University, New Haven, CT

6. Faculty of Medicine, University of Ottawa, Ottawa, Canada

7. NYU Neuroscience Institute, New York University, New York, NY 10016

*to whom communication should be addressed: edward.ruthazer@mcgill.ca

Keywords: Xenopus, retinotectal, TrkB, $p75^{NTR}$, retinal ganglion cell, axon, activity-dependent, in vivo imaging

Summary

During development, patterned neural activity in input neurons innervating their target, instructs topographic map refinement. Axons from adjacent neurons, firing with similar patterns of neural activity, converge onto target neurons and stabilize their synapses with these postsynaptic partners (Hebbian plasticity). On the other hand, non-correlated firing of inputs promotes synaptic weakening and exploratory axonal growth (Stentian plasticity). We used visual stimulation to control the visually-evoked correlation structure of neural activity in ectopic ipsilaterally projecting (ipsi) retinal ganglion cell axons with respect to their neighboring contralateral eye inputs in the optic tectum of albino *Xenopus laevis* tadpoles. Multiphoton imaging of the ipsi axons in the live tadpole, combined with manipulation of brain-derived neurotrophic factor (BDNF) signaling, revealed that presynaptic $p75^{NTR}$ and TrkB both promoted axonal branch addition during Stentian plasticity, whereas predominantly postsynaptic BDNF signaling mediated activity-dependent Hebbian suppression of axon branch addition. Additionally, we found that BDNF signaling is required for local suppression of branch loss induced by correlated firing.

Introduction

Sensory experience during early development is crucial for the formation of precise topographic maps throughout the brain (López-Bendito and Molnár, 2003). Retinal ganglion cells (RGCs) in fish and amphibians fire action potentials in response to visual stimuli as they extend into the optic tectum (Demas et al., 2012; Holt and Harris, 1983). Therefore, temporal correlation in firing patterns of RGCs is indicative of their mutual proximity in the retina and the developing visual system uses this information to instruct structural and functional refinement of retinotopic and eye-specific maps (Zhang et al., 2011; Munz et al., 2014; Kutsarova et al., 2016). Concretely, co-activation of RGC inputs, read out by calcium flux through postsynaptic N-methyl D-aspartate receptors (NMDARs), stabilizes retinotectal synapses and their axonal arbors. This correlation-dependent stabilization is called “Hebbian plasticity.” In contrast, asynchronous firing of RGC axons with respect to their neighboring inputs leads to synaptic weakening, accompanied by an increase in axonal branch dynamics and exploratory growth, presumably aiding axons to seek out more appropriate postsynaptic partners (Hebb, 1949; Stent, 1973; Cline et al., 1987; Rajan et al., 1999; Ruthazer et al., 2003; Mu and Poo, 2006; Munz et al., 2014; Kesner et al., 2020;). This is referred to as “Stentian plasticity”, and recent evidence indicates that it is the unaccompanied firing of neighboring inputs that promotes Stentian growth of axons that have not been stabilized by correlated firing and NMDAR activation (Rahman et al., 2020). Brain-derived neurotrophic factor (BDNF) has been implicated as a potent modulator of synaptic and structural plasticity throughout the brain (Zagrebelsky and Korte, 2014). BDNF can be synthesized and released in a constitutive or activity-dependent manner from axonal terminals and dendrites (Mowla et al., 1999; Balkowiec and Katz, 2000; Yang et al., 2009: Dieni et al., 2012; Orefice et al., 2016; Vignoli et al., 2016). It can be released as an active precursor form, proBDNF, which exerts its function mainly via $p75^{NTR}$ and sortilin signaling, or as the cleaved mature form (mBDNF), which signals mainly via TrkB and $p75^{NTR}$/TrkB (Chao and Hempstead, 1995; Rösch et al., 2005; Woo et al., 2005; Baho et al., 2019). The specifics of BDNF synthesis, secretion and receptor signaling create multi-layered regulation underlying the diversity of functions served by BDNF in the brain. Notably, at developing neuromuscular synapses, proBDNF signaling through

presynaptic p75^{NTR} is required for axonal retraction, whereas mBDNF signaling through presynaptic TrkB leads to axonal stabilization (Je et al., 2012, 2013). In the developing retinotectal system, exogenous application of BDNF induces RGC axon branching and growth, whereas depletion of endogenous BDNF impedes presynaptic synaptobrevin punctum and axonal branch stabilization (Alsina et al., 2001; Cohen-Cory and Fraser, 1995; Hu et al., 2005; Marshak et al., 2007). BDNF signaling through the TrkB receptor is necessary for Hebbian synaptic strengthening induced by visual conditioning in the Xenopus retinotectal system, whereas proBNDF signaling through p75^{NTR} facilitates synaptic weakening (Mu and Poo, 2006; Schwartz et al., 2011).

To test what aspects of BDNF signaling are respectively involved in Hebbian and Stentian structural plasticity, we took advantage of the occasional presence of ectopic ipsilaterally projecting (ipsi) RGC axons in the optic tectum of developing albino *Xenopus laevis* tadpoles (Munz et al., 2014). These ipsi axonal projections, which typically consist of just one or two ectopic axons, occur in fewer than half of all animals. Exploiting the presence of an ipsi axon, we used a fiber optic to present light to one eye, visually stimulating the ipsi axon in or out of synchrony with the other eye, from which the bulk of neighboring, contralaterally projecting RGC inputs originates. Furthermore, by electroporating one eye with antisense Morpholino oligonucleotides (MO) we were able to selectively knock down components of BDNF signaling in these ipsi axons. In this study, we provide *in vivo* imaging evidence for the involvement of presynaptic p75^{NTR} and TrkB receptors as positive regulators of Stentian axonal branching and growth, whereas Hebbian branching suppression signals were blocked by systemic inhibition of BDNF signaling. Our data further demonstrate that BDNF signaling acts locally to protect axonal branches from elimination.

Results

Stentian and Hebbian structural plasticity are mediated by distinct components of BDNF signaling

We performed *in vivo* 2-photon imaging of EGFP-expressing ipsi RGC axonal arbors in the optic tectum every 10 min for up to 5 h while subjecting the animals to a Darkness-Asynchronous-Synchronous (DAS) visual stimulation protocol (**Figures 1A and 1B**).

This protocol had been used in a previous study to reveal that ipsi RGC axons exhibit greater branch dynamics and arbor growth when stimulated asynchronously relative to surrounding contra RGC inputs, but this dynamic branching behavior is suppressed by correlated synchronous activation of the ipsi and contra axons resulting in arbor stabilization (Munz et al., 2014). To alter BDNF signaling, we employed two strategies: either intraventricular injection of TrkB-Fc to sequester BDNF acutely, or co-electroporation of EGFP with antisense morpholino oligonucleotide (MO) against $p75^{NTR}$ or TrkB in the eye to achieve presynaptic knock-down of these receptors in the RGC (**Figure 1A, Figure S1**). MOs were tagged with the red fluorescent dye lissamine which filled the entire RGC out to its axonal terminal, permitting knock-down in individual axons to be confirmed by the presence of both EGFP and lissamine fluorescence. We quantified the numbers of newly added and lost branches per axon for each 10 min imaging interval throughout the DAS protocol (**Figures 1B and 1C**). Ipsi axons containing Ctrl-MO (Control) exhibited increased branch additions during asynchronous stimulation of the two eyes compared to synchronous stimulation (**Figures 1D and 1F**) in line with a previous report (Munz et al., 2014). In p75-MO and in TrkB-MO ipsi axons, the increase in branch additions induced by asynchronous stimulation was prevented (**Figures 1D and 1F**), indicating a direct role of neurotrophin receptor activation in Stentian plasticity.

On the other hand, the Hebbian suppression of new branch additions during synchronous binocular stimulation (Munz et al., 2014) was prevented by depletion of BDNF signaling by extracellular application of TrkB-Fc (**Figures 1D and 1F**). The significant increase in branch additions during synchronous stimulation exclusively in TrkB-Fc treated, but not in neurotrophin receptor MO animals, suggests a key role for BDNF release or extracellular processing in Hebbian suppression of branch addition. Interestingly, we observed significantly higher rates of branch addition during synchronous stimulation in BDNF depleted tecta, compared to presynaptic $p75^{NTR}$ or TrkB knock-down, implying that BDNF acts on targets other than the axon itself, presumably the postsynaptic terminal, to induce retrograde signals that inhibit formation of new axonal branches.

Presynaptic BDNF signaling helps suppress branch loss during stimulation

In the OT, RGC axons, their postsynaptic partners, and surrounding glia, all rapidly extend and retract their processes during structural refinement of the developing retinotopic map. Axonal branch elimination occurs in parts of the arbor where synapses have failed to undergo stabilization, permitting axon pruning and topographic map refinement (Kutsarova et al., 2016). Knock-down of $p75^{NTR}$ or TrkB in the ipsi RGC axon, as well as broad depletion of BDNF signaling, led to an overall increase in the rates of axonal branch loss in response to visual stimulation compared to control ipsi axons (**Figures 1E and 1G**). Thus, under normal conditions, BDNF signaling can help stabilize axons against activity-induced axonal branch loss.

BDNF signaling spatially restricts branch elimination events

Previous studies have shown that new axonal branches emerge more readily from sites bearing pre-existing synapses, and consequently stable synapses can nucleate further branch extension (Haas et al., 2006; Meyer and Smith, 2006; Ruthazer et al., 2006). Retraction of axonal branches is halted at sites carrying mature synapses, suggesting that branches with strong synaptic contacts are more likely to be spared from elimination. These findings point to targeted arbor growth as well as synaptotropic constraints in arbor elimination (Cline and Haas, 2008). Interestingly, local action of BDNF has previously been shown to alter synaptic maturation and dendritic morphology in cells within close proximity to release sites (Horch and Katz, 2002; Ohba et al., 2005; Zhang and Poo, 2002; Kohara et al., 2007). We set out to further explore the role of BDNF signaling in the spatial organization of axonal branch addition and elimination events in response to patterned activity (**Figures 2A and 2B**). To assess whether remodeling events occurred in close proximity to each other, indicative of local signaling on the arbor, we extracted the pairwise distances for all addition and for all elimination events during darkness, asynchronous and synchronous stimulation (**Figure 2C**) and calculated a mean event pair distance for each stimulation period (**Figure 2D**), shown for the example axon (Figure 2C). Differences in arbor size and shape may impact measurements of mean event pair distance. We therefore performed Monte Carlo simulations of the locations of events on the arbor (**Figure S2**) and used the simulated

mean event pair distances to correct for differences in arbor morphology for all analyses. The corrected mean pairwise distance between elimination events was significantly lower during synchronous stimulation compared to darkness in control axons, consistent with fewer branch elimination events occurring far apart from each other during correlated firing induced by synchronous stimulation (**Figures 2D and 2E**). These data reveal that correlated activity causes branch eliminations to become restricted to a relatively smaller portion of the total arbor, likely through the local stabilization of some branches. Extracellular depletion of BDNF with TrkB-Fc, or knock-down of $p75^{NTR}$ or TrkB in ipsi axons, resulted in a redistribution of branch elimination events that no longer favored the proximity of events normally seen with synchronous stimulation (**Figure 2E**). Interestingly, this spatial phenomenon was limited to branch elimination, as we observed no difference in mean pairwise distances of addition events in control axons (**Figure 2F**) across the stimulation periods. These findings point to a model in which secreted neurotrophin appears to influence branch eliminations and stabilization within spatially constrained local zones of action.

Axon arbor elaboration over days relies on $p75^{NTR}$ expression in the RGCs

Retinotectal axon arbors remodel over a period spanning several days under the influence of ongoing sensory input. We followed the elaboration of individual RGC axons from the contralateral eye in the optic tectum over 4 days, by co-electroporating EGFP together with either p75-MO or TrkB-MO to assess the roles played by these receptors in arbor remodeling (**Figures 3A-C**). Interestingly, RGC axons knocked down for $p75^{NTR}$ exhibited a decreased accumulation of branch tips compared to axons electroporated with TrkB-MO (**Figures 3D and 3E**), suggesting that $p75^{NTR}$ promotes axonal branch elaboration. Furthermore, $p75^{NTR}$ knock-down also resulted in a significant decrease in the axonal skeletal length compared to control axons (electroporated with Ctrl-MO) and RGCs electroporated with TrkB-MO (**Figure 3F**), pointing to a major role for $p75^{NTR}$ in axonal arbor growth. In addition, binning terminal segments (**Figure 3D**) by length revealed that as axonal arbors became more complex over 4 days, the proportion of terminal segments categorized as short (1-5 µm) decreased in control and TrkB-MO axons, whereas it remained unchanged in the p75-MO axons, consistent with their failure

to undergo progressive elaboration (**Figure 3G**). These data reveal that p75^{NTR} in the RGCs helps both to promote new branch accumulation and the elongation of the short filopodium-like branches over days, resulting in a more complex terminal arbor.

p75^{NTR} and TrkB in RGCs play opposing roles in axonal arbor span enlargement

Upon entry into the OT, RGC axons exhibit simple morphologies, possessing few branches and a prominent terminal growth cone. As they grow toward their termination zone in the OT, arbors increase in complexity, which is reflected in increases in the number of terminal points, the total skeleton length, and the span of the arbor (**Figures 3 and 4**). In general, conditions that increase these measures of RGC axonal arbors are typically accompanied by increased tectal receptive field size and decreased visual acuity (Rossi et al., 2001; Mrsic-Flogel et al., 2005; Smear et al., 2007; Dhande et al., 2011). The retinotopic map occupies a 3D volume within the OT, and consequently a more relevant metric of an axon's morphology should be the volume of its arbor span. We calculated arbor span volume by obtaining a measure of the convexity of the 3D reconstructed axonal arbor, which was used to define an enclosing volume whose border lies between a tight fit and a convex hull around the arbor, as described by Bird and Cuntz (2019) (**Figures 4A-C**). We found that knock-down of p75^{NTR} and TrkB in RGCs resulted in opposite changes in arbor span volume, with TrkB-MO arbors expanding more rapidly over 4 days to occupy a greater volume in the optic tectum compared to p75-MO axons (**Figure 4D-E**). These observations suggest that p75^{NTR} in the RGC promotes enlargement of the axonal arbor span volume, whereas TrkB impedes the expansion of RGC arbor volume.

Discussion

Presynaptic p75^{NTR} and TrkB in Stentian exploratory growth

We have shown that presynaptic knock-down of p75^{NTR} and TrkB receptors blocks the Stentian increase in new branch addition that occurs when an axon does not fire in synchrony with its neighbors (**Figures 1D and 1F**) (Munz et al., 2014; Rahman et al., 2020). Furthermore, we found a decrease in branch tip accumulation over 4 days of repeated imaging in p75-MO axons (**Figure 3E**). A role for p75^{NTR} in the process of

exploratory growth is supported by our finding that p75^{NTR} promotes the elongation of axonal branches specifically through the extension of the shortest filopodium-like branches (**Figure 3G**). Previous work has revealed that when inputs surrounding an axon actively fire while that axon is quiescent, Stentian "exploratory growth" of the inactive axon takes place, suggesting the release of an intercellular growth-promoting signal by neighboring cells in the optic tectum (Rahman et al., 2020). In our paradigm, the p75-MO is electroporated only in the ipsi eye, and not in the neighboring axons in the tectum which come from the other eye, implying that it is p75^{NTR} specifically on the asynchronously firing RGC axon which responds to the Stentian signals that promote branch addition and extension. Putative p75^{NTR} ligands could be released directly by the neighboring axons, indirectly by the postsynaptic neurons or even by local glia. Further investigation is required to reveal the identities and the exact sites of release of the potential ligands. However, proBDNF-induced activation of p75^{NTR} has been shown to promote synaptic weakening both in *Xenopus* tadpoles and in mice (Woo et al., 2005; Schwartz et al., 2011; Winnubst et al., 2015), consistent with prior reports that exploratory growth is accompanied by a marked reduction in synaptic strength (Munz et al., 2014). Injection of BDNF in the optic tectum drives a robust increase in RGC axonal branch number, an effect which could potentially be the result of activation of either TrkB or p75^{NTR} (Cohen-Cory and Fraser, 1995). In addition, NT3 is another p75^{NTR} ligand which has been linked specifically to the addition of short filopodium-like branches. The molecular mechanisms following p75^{NTR} activation may differ in the somato-dendritic and the axonal compartments due to differential expression of p75^{NTR} interacting partners (Hermey et al., 2001; Wang et al., 2002; Bronfman and Fainzilber, 2004). Activation of dendritic p75^{NTR} has been shown to result in a reduction in dendritic branch complexity and dendritic spine density in rodent hippocampal neurons (Yang et al., 2014; Orefice et al., 2016). In contrast, our data demonstrate that *Xenopus* retinotectal axons exhibit Stentian exploratory growth in response to p75^{NTR} activity.

In the daily imaging data of contralaterally projecting axons, knock-down of TrkB exerted little effect on axonal arbor branch accumulation and elongation over days (**Figure 3**). It is crucial to consider, however, that during their normal development, RGC axons are directed by gradients of molecular guidance cues to their approximate

topographic termination zones in the optic tectum and thus, on average should exhibit a pattern of firing that is relatively correlated with that of their neighbors (McLaughlin et al., 2003). It is therefore plausible that this level of correlated neural activity obscures the effects of Stentian plasticity on axonal growth over days. The short-term dynamic imaging of ipsi axons, which allowed us to systematically and drastically alter the degree of correlation in RGC firing, unmasked a role for presynaptic TrkB in contributing to Stentian structural plasticity through an increase in the rate of new branch addition (**Figures 1D and 1F**).

BDNF signaling in Hebbian suppression of axonal branch addition

The axonal branch stabilization induced by correlated firing is dependent on the activation of NMDARs (Ruthazer et al., 2003; Munz et al., 2014). Specifically, postsynaptic knock-down of NMDARs in optic tectal neurons results in an increased number of branch tips in RGC axons, suggesting the existence of a putative retrograde signal that promotes presynaptic axonal arbor stabilization (Kesner et al., 2020). In addition, such retrograde signaling appears to depend on the activation of CaMKII in the optic tectal neurons (Zou and Cline, 1996). Sequestering extracellular BDNF prevented the decrease in branch additions during synchronous stimulation in our experiments involving dynamic imaging of ipsi axons, a result that was not replicated by axonal p75-MO or TrkB-MO, suggesting that BDNF indirectly mediates axonal stabilization, perhaps by acting postsynaptically to drive release of the putative retrograde signal (**Figures 1D and 1F**). It is also plausible that BDNF may be released downstream of postsynaptic NMDAR activation and act as an autocrine signal mediating synaptic strengthening (Schwartz et al., 2011; Harward et al., 2016; Vignoli et al., 2016).

Our data provide evidence for BDNF acting presynaptically to promote Stentian exploratory branching and postsynaptically to drive Hebbian stabilization that results in suppression of new branch addition. These opposing effects could reflect differences in the levels of expression of TrkB and $p75^{NTR}$ and their interactors in dendrites and axons as previously mentioned (Dougherty and Milner, 1999; Hermey et al., 2001; Wang et al., 2002; Bronfman and Fainzilber, 2004). Another possibility is that proBDNF may be released in response to neural activity to act on $p75^{NTR}$, but can be further converted to

mBDNF through NMDAR-dependent activation or release of tissue plasminogen activator (tPA) or matrix metaloproteinase-9 (MMP-9), leading to preferential activation of TrkB during synchronous stimulation (Qian et al., 1993; Pang et al., 2004; Dziembowska et al., 2012). Moreover, tPA has been implicated in synaptic strengthening in the retinotectal projection in response to visual conditioning (Schwartz et al., 2011). There is evidence to suggest that MMP-9 is involved in the processing of proBDNF to mBDNF leading to stabilization of a robustly firing motor axon in the NMJ, or in strengthening of co-active synapses in the CNS (Je et al., 2012; Niculescu et al., 2018). In the *Xenopus* OT, MMP-9 is necessary for the visual experience driven increase in tectal neuron dendritic growth (Gore *et al.*, 2021). Recent results from computational modeling suggest that the ratio of proBDNF/mBDNF, regulated by local action of MMP-9, combined with a precisely-timed rise in postsynaptic calcium may be crucial to switch plasticity from depression to potentiation, presumably due to preferential activation of $p75^{NTR}$ and TrkB, respectively (Kirchner and Gjorgjieva, 2021). It is also plausible that the mode of BDNF release varies during asynchronous and synchronous stimulation, in line with reports proposing that tonic versus acute release of BDNF may differentially regulate the cell surface level of TrkB and thus distinctly affect neurite outgrowth (Haapasalo et al., 2002; Ji et al., 2010; Guo et al., 2018).

Local action of BDNF signaling in Hebbian branch stabilization

Our analyses on the spatial distributions of addition and elimination of axonal branches revealed that correlated firing led to more locally targeted elimination events compared to what occurs in darkness, whereas the mean distance between addition events stayed similar regardless of stimulation (**Figures 2D-F**). These data are consistent with previous observations in tadpoles with binocularly innervated optic tecta showing that axonal branches are added uniformly across the arbor, but branch loss tends to occur in the territory where inputs from the opposite eye dominate (Ruthazer et al., 2003). Targeted axonal branch loss within restricted parts of the arbor is consistent with the existence of widespread elimination-inducing signals counteracted by locally diffusible signals that protect axonal branches from being eliminated in certain parts of the arbor. We found that disrupting BDNF signaling in the retinotectal system resulted in

increased rates of branch elimination (**Figure 1E and 1G**). Our data suggest that local release of BDNF locally confers axonal branch stabilization, such that blocking BDNF signaling increases the probability of randomly occurring elimination events under conditions of correlated neural activity. Altering the spatial distribution of elimination events over longer time periods should lead to less compact arbors. Indeed, we observed that TrkB knock-down in RGCs led to a notably enlarged axonal arbor span (**Figure 4**). This effect on arbor span was not seen in $p75^{NTR}$ knock-down axons, most likely due to their overall reduced arbor length and branch number.

In summary, the visual stimulation paradigm in these experiments allowed us to reveal that distinct aspects of BDNF signaling are responsible for Stentian and Hebbian structural plasticity during development (**Figures 4F-H**). We propose that presynaptic $p75^{NTR}$ and TrkB signaling promote aspects of Stentian exploratory growth (**Figure 4G**) in response to asynchronous activity. On the other hand, BDNF signaling, most likely acting postsynaptically, is necessary for the Hebbian suppression of branch addition and acts locally within the arbor to regulate axonal branch loss that occurs during correlated firing (**Figure 4H**).

Acknowledgements

We thank Kurt Haas (UBC) for Dynamo software, Kelly Sakaki (UBC) for ideas on imaging setup, Peter Donhauser (ESI) for discussions on image and statistical analysis, Tasnia Rahman (McGill) and Philip Kesner (McGill) for experimental blinding. Funding sources are Jeanne Timmins Costello and Molson Neuroengineering Studentships (E.K.), Ann and Richard Sievers Award in Neuroscience (M.M.), McGill SURA (A.W.), CIHR Foundation Grant (FDN-143238; E.S.R.) and NSERC CREATE Neuroengineering Training Grant (E.S.R).

Author Contributions

E.K., A.S., MM. and E.S.R. conceived the experiments. E.K. and A.S. developed the methodology and generated resources. E.K., A.S., M.M., Y.Y.Z., A.W., O.M.B performed experiments. E.K. analyzed the data. E.K. and E.S.R. drafted the manuscript. All authors provided critical feedback and editing of the final manuscript. E.S.R. secured funding and supervised the project.

Declaration of Interests

The authors declare no competing interests.

Resource availability

Lead Contact

Further information and requests for resources and reagents should be directed to and will be fulfilled by the lead contact, Edward S. Ruthazer (edward.ruthazer@mcgill.ca).

Materials Availability

Any reagents generated for this study will be made available upon request to the lead contact. Alternatively, the requestor will be directed to a public repository tasked with distributing the reagent.

Data and Code Availability

Any code and original data generated in this study will be made freely available upon request to the lead contact. Custom MATLAB software (CANDLE denoising) used in this study is available for free download at https://sites.google.com/site/pierrickcoupe/softwares/denoising-for-medical-imaging/multiphoton-filtering

Experimental model and subject details

The experiments described in this study were approved by the Animal Care Committee at the Montreal Neurological Institute and are in accordance with the guidelines of the Canadian Council on Animal Care. Animals of both sexes were used for the experiments; At the stages of interest for our study, the sexes cannot be distinguished anatomically. Albino *Xenopus laevis* tadpoles were generated by induced mating of a sexually mature female frog, injected with pregnant mare serum gonadotropin (50 IU) 3 days before mating and with 400 IU human chorionic gonadotropin (HCG) immediately before mating, and a sexually mature male frog injected with 150 IU HCG up to 8 hours before mating. The produced fertilized eggs were reared in 0.1X modified Barth's saline with HEPES (MBSH).

Method details

Morpholino Oligonucleotides

Xenopus p75^{NTR} morpholino sequence: 5′-CCA TGC TGA TCC TAG AAA GCT GAT G-3′ , referred to as p75-MO, *Xenopus* TrkB morpholino sequence: 5′-CCA CTG GAT CCC CCC TAG AAT GGA G-3′ (Du and Poo, 2004; Je et al., 2012), referred to as TrkB-MO, and standard control: 5'-CCT CTT ACC TCA GTT ACA ATT TAT A 3' (Gene Tools, LLC), referred to as Ctrl-MO, were generated and tagged with lissamine on the 3'-end (Gene Tools, LLC).

TrkB-MO validation experiments

Albino *Xenopus laevis* embryos were microinjected at the 2-cell stage with 18 ng of Morpholino (TrkB-MO or Ctrl-MO) in each blastomere, using an automatic pressure

microinjector (Harvard Apparatus) with micropipettes pulled from glass (6.66 µL, Drummond Scientific), using a Flaming Brown Micropipette Puller (P-97, Sutter Instruments CO.). The morphant tadpoles were screened for lissamine fluorescence at st. 46 (Nieuwkoop and Faber, 1994). Aside from one phospho-Trk antibody (Cell Signalling, 9141, AB_2298805), the antibodies against TrkB that we tested showed lack of specificity to the *Xenopus laevis* TrkB. We therefore validated the TrkB-MO by measuring the level of phospho-TrkB in response to BDNF treatment between animals injected with Ctrl-MO and TrkB-MO using the phospho-Trk antibody.

Stage 46 *Xenopus laevis* tadpoles injected at the 2-cell stage with TrkB-MO or Ctrl-MO and positive for lissamine fluorescence were injected intraventricularly with 100 ng/µL BDNF (B-250, Alomone Labs) using the same setup described for electroporation-related DNA injections. After 1 h, brains were dissected and extracted in NP-40 extraction buffer (10 mM HEPES/NaOH pH 7.4, 150 mM NaCl, 2 mM EDTA pH 8.0, 1% NP40) with Halt™ protease/phosphatase inhibitor cocktail (ThermoScientific, P178442). Brain extracts were then homogenized using 10 s continuous 10% Amplitude on a Branson 250 Sonifier (Branson Ultrasonics™) equipped with a microtip. The extracts were centrifuged at 13,000 rpm at 4ºC for 10 min using a Biofuge 13 centrifuge (Heraeus Instruments). Laemmli sample buffer (50 mM Tris/HCl pH 6.8, 10% Glycerol, 2% SDS, 0.025% Bromphenol Blue, 100 mM DTT) was added to the supernatant and the protein samples were then boiled at 100°C for 5 min for reduction and denaturation of the protein structure. Proteins were separated on SDS-PAGE (8%) transferred to PVDF membranes (Immobilon-P, 0.45 µm, Millipore) using wet transfer in transfer buffer (48 mM Tris base, 39 mM glycine, 0.037% SDS, 20% methanol). Molecular markers of known size (Precision Plus Protein™ Dual Color Standard, Bio-Rad) were run in parallel with the proteins of interest. Blots were probed with 1:5,000 rabbit anti-p-Trk (Cell Signalling, 9141, AB_2298805), 1:10,000 peroxidase AffiniPure Goat AntiRabbit IgG (H+L; Jackson Immuno Research Laboratories, inc., 111-035-144, AB_2307391) was used for visualization. Blots were blocked using 5% BSA (Fraction V, Fisher Scientific) in TBS-T (20 mM Tris/HCl pH 7.6, 135 mM NaCl, 0.05% Tween) for p-Trk, and with 5% fat-free milk in TBS-T for β-tubulin. To ensure equal loading the blots were probed with 1:20,000 rabbit anti-β-tubulin (sc-9104, Santa Cruz Biotechnology, AB_2241191) and 1:20,000

peroxidase AffiniPure Goat AntiRabbit IgG. Immobilon™ Western Chemiluminescent HRP Substrate (Millipore) was used to visualize the protein bands on the blots, diluted 1:1 in double distilled water. HyBlot Autoradiography films (Denville Scientific, Inc.) were used to collect images of the protein bands.

p75-MO validation experiments

Due to a lack of *Xenopus laevis* $p75^{NTR}$-specific antibody, we took an indirect route to validate that the p75-MO knocks down *Xenopus laevis* $p75^{NTR}$. The $p75^{NTR}$ sequence was cloned from cDNA from st. 24 *Xenopus laevis* tadpoles (Nieuwkoop and Faber, 1994) Total RNA was extracted from st. 24 tadpoles and cDNA was transcribed with Superscript IV (Thermo Fisher, 18090010). The coding sequence (cds) of $p75^{NTR}$ (starting from the ATG, insensitive to the morpholino, MOres-$p75^{NTR}$) and the cds with part of the 5'UTR (nucleotide -29 from ATG, sensitive to the morpholino, $p75^{NTR}$) were PCR amplified using the following forward primers: MOres-$p75^{NTR}$: 5' ACG TGA ATT CAT GGA AAC CCC TCT G 3', p75NTR: 5' ACG TGA ATT CCC TCA GCC ATC AGC T 3'. The reverse primer was the same for both sequences, $p75^{NTR}$-reverse: 5' ACG TAC CGG TAA CAC GGG TGA GGT A 3'. The PCR fragments were cloned in frame with EGFP into pCS2+ vector, resulting in MOres-p75-EGFP and p75-EGFP. The plasmids were linearized with NotI and mRNA was prepared with the SP6 mMessageMachine kit (Thermo Fisher, AM1340). Animals were injected at the early 2-cell stage with 2 x 200 pg of either MOres-p75-EGFP or p75-EGFP followed by injection of 2 x 18ng of p75-MO. Animals were screened for MO (lissamine) and EGFP expression. In the animals expressing p75-EGFP and p75-MO there was hardly any EGFP visible and lissamine was used to select animals. Whole animals were extracted at st. 26 in NP40 extraction Buffer supplemented with Halt™ protease/phosphatase inhibitor cocktail (ThermoScientific, P178442). Samples were incubated with Laemmli Buffer for 20 min at 37˚C. Extracts were separated on 8% SDS-PAGE (as described in TrkB-MO validations experiments), transferred to PVDF membrane and subsequently stained for EGFP (anti-GFP antibody, 1:20000, abcam ab13970, AB_300798) and goat anti-chicken HRP 1:10,000 (Jackson Immuno Research Laboratories, inc., 103-035-155, AB_233738) and β-tubulin (anti-β-tubulin, 1:20,000,

Santa Cruz sc-9104, AB_2241191) and AffiniPure Goat AntiRabbit IgG 1:20,000, as a loading control. Blots were imaged on a BioRad ChemiDoc Imaging System.

Sparse labeling of contralaterally or ipsilaterally projecting RGC axons

Albino *Xenopus laevis* tadpoles (stages 40-42) were anaesthetized by immersion in 0.02% MS-222 (Sigma, A5040) diluted in 0.1X MBSH. The developmental stages were determined using the standard criteria of Nieuwkoop and Faber (1994). EGFP DNA plasmid (pEGFP-N1, Clonetech, 6085-1) and oligonucleotides were pressure-injected into the eye using micropipettes pulled from borosilicate glass with filament (outer diameter 1.0 mm, inner diameter 0.78 mm; Sutter Instruments) on a PC-10 puller (Narishige, Japan) and attached to a custom-built manual pressure injection system. Upon pressure injection of plasmid/morpholino solutions into the eye, current was delivered across two custom-made platinum plates placed in parallel. A Grass 9 constant voltage stimulator with a 3 μF capacitor placed in parallel was used to deliver 2 pulses in each direction: 1.6 ms duration, 36 V for contra axons, 2.5 - 3 ms, 36 V for ipsi axons. After electroporation, the animals were placed in a 20ºC biological oxygen demand incubator in a 12h light/12h dark cycle. For long-term daily imaging of contra RGC axons, RGCs were co-electroporated with MO and plasmid encoding EGFP (4.5 μg/μL : 1.5 μg/μL). To express EGFP in ipsi RGC axons, 2 μg/μL plasmid was pressure-injected. For experiments involving ipsi knock-down of the BDNF receptors solution containing 3 μg/μL : 4 μg/μL MO and EGFP was injected into the eye in order to achieve efficient co-delivery

Daily imaging of morpholino-loaded/EGFP expressing RGC axons

Animals at st. 45-46 (3 days post-electroporation) containing a single co-labeled RGC axon were selected and imaged over the next 4 days. After anaesthetizing the tadpoles by immersion in 0.02% MS-222 (Sigma, T2379) in 0.1x MBSH, they were positioned in custom-made polydimethylsiloxane (PDMS) imaging chambers. Optical section z-series at 1 μm steps of the axons of interest were acquired using an Olympus FV300 confocal microscope converted for multiphoton use, equipped with a 60x LUMPlanFL N 1.0NA water immersion objective. For optimal excitation of the axon-filling EGFP, imaging was carried out at 910 nm once every day for 4 days. To confirm the presence of lissamine-tagged MO in the axons of interest and assure minimal cross-talk between the two

channels (green: 500-550 nm and red: 593-668 nm) 3D fluorescence stacks were also acquired at 840 nm where the EGFP excitation is minimal and the lissamine excitation peaks.

Dynamic imaging of ipsilaterally projecting RGC axons combined with visual stimulation

Animals were given at least 4 days post-electroporation to assure labeling and proper knock-down in ipsi axons and imaging was performed in stage 47-48 tadpoles. The animals were immobilized by intraperitoneal injection of 2.5 mM tubocurarine hydrochloride pentahydrate (Sigma). In the experiments including acute pharmacological blockade, 50 µg/mL TrkB-Fc (Recombinant Human Chimera, 688-TK, R&D Systems) was injected intraventricularly. The animals were then placed in a custom-built imaging chamber (PDMS), fixed in place with a small drop of 1.8% UltraPureTM Low Melting Point Agarose (Invitrogen, 16520). The imaging chamber contains two channels for fiber optics, one leading to each eye, a perfusion and spillover chambers, as previously described (Rahman et al., 2020). During the whole imaging session, the tadpoles were perfused with O_2-bubbled 0.1x MBSH. Light flashes were delivered separately to each eye using an FG365LEC-Custom optic fiber (ThorLabs) placed in a channel leading to each eye. To generate light flashes Red Rebel 102lm@700mA LEDs (Luxeon Star, Ltd) controlled by STG4002 and MC Stimulus-II software (Multichannel Systems) were used. After stabilizing the tadpoles, the chamber was placed under the two-photon microscope where the animals habituated in darkness for 30 min. Optical section z-series at 1 µm steps of the EGFP-labeled ipsi axons were acquired every 10 min for 1 h in darkness followed by 1.5 h of asynchronous stimulation: 10 ms flashes, alternating between the two eyes at a duty cycle of 0.5 Hz for each eye, followed by 1.5 h of synchronous stimulation: simultaneous 10 ms flashes light in the two eyes presented at 0.5 Hz. For some experiments involving knock-down of proteins of interest, optical section z-series of EGFP and lissamine co-labeled RGC axons were acquired for 1 h in darkness, 2 h in asynchronous and 2 h in synchronous stimulation. Imaging was performed at 910 nm allowing optimal excitation of EGFP using a ThorLabs multiphoton microscope equipped with XLUMPlanFL N 1.0 NA 20x WI objective (Olympus), two channels with gallium arsenide phosphide photo-multiplier tubes (GaAsP PMTs) filtered to detect green and red emission (525/50 and 630/92) and ThorImage software. For some experiments including

co-electroporation of EGFP and MO, additional optical section z-series were collected at the end of each imaging session at 840 nm to ensure minimal excitation of EGFP and maximal excitation of lissamine.

Quantification and statistical analysis

Image Analysis

All multiphoton z-series were denoised using CANDLE software implemented in MATLAB (MathWorks) which relies on non-local mean filtering methods (Coupé et al., 2012). Denoised 3D stacks were then used to reconstruct axonal arbors using “Autopath” and “Autodepth” features in Imaris 6.4.2 (Bitplane) for daily imaging experiments and by manual tracing in Dynamo software (Munz et al., 2014), implemented in MATLAB (MathWorks), generously provided by Drs. Kaspar Podgorski and Kurt Haas (UBC). For morphometric analysis of daily imaged RGC axonal terminal branch points were extracted from Imaris 6.4.2. PyImarisSWC Xtension, implemented in Python, installed in Imaris 9.5.1, was used to export the Imaris reconstructions as swc-files. The exported node coordinates were converted from pixel to µm. The swc-files were imported using “trees toolbox” (Cuntz et al., 2010), which was used to classify axonal segments according to their order derived by the Strahler ordering method, using “strahler_tree” function (Strahler, 1957; Uylings et al., 1975; Vormberg et al., 2017). Axonal segments are defined as axonal structure bordered by two branch points or by a branch and a terminal point. The length of axonal segments with Strahler number of one, referred to as terminal segments was extracted and the distribution of terminal segments binned by length was followed over 4 days. The length of all segments with Strahler number>1 was counted toward the total skeleton length. Axonal span volume was calculated after obtaining the convexity of the 3D reconstructed arbors with “convexity_tree” function and then using the value to calculate and feed a shrink factor into “boundary_tree” function of “tree toolbox” as described by (Bird and Cuntz, 2019). From the dynamic imaging experiments ipsi RGC axon branch additions and eliminations between two consecutive time-series (10 min) were extracted and further normalizations were performed as described in each individual case in the figure legends. A branch was counted towards any further analysis only if it attained a length of 1.5 µm at some point during the imaging session. Addition

events were defined as the branch points of newly added branches between “t-10 min” and “t”. Elimination events were defined as the terminal points of branches lost between “t” and “t+10 min”. Rigid body transformation using manual landmarks in Dynamo was applied to align the timepoints of the reconstructed arbor. The coordinates of all the events throughout a stimulation period – dark, asynchronous or synchronous, were extracted and the pairwise distances between all the elimination and all the addition events were calculated. For one axon from the TrkB-Fc group, there was only one elimination event throughout the dark period, which prevented the calculation of mean elimination event pair distance for the dark period and further normalization. Thus, this cell was excluded from the elimination event analyses. To assess whether the changes in mean distances were explained by changes in axon arbor morphology, a randomization of the events on the axonal arbor was performed. To do that, the reconstructions in Dynamo were used to extract the coordinates of each node and a swc-file was exported for each timepoint of the imaging session. The reconstruction was then resampled using “resample_tree” from “trees_toolbox” such that the nodes composing the arbor were equidistant at 0.15 µm. The number of observed addition events between “t-10 min” and “t” was randomly distributed on the axonal arbor at “t”. The number of observed elimination events between t” and “t+10 min” was randomly assigned to the terminal points of the axonal arbor at “t”. Pairwise distances between the simulated addition or elimination events within a stimulation period was calculated and then the mean pairwise distance for stimulation period obtained. This randomization was repeated 100 times and the average simulated mean pairwise distance plotted on **Figure S2**. The ratio of the observed and simulated mean pairwise distance was plotted on **Figure 2E-F**. The imaging experiments and the axonal reconstructions were performed blind to the experimental design, except for one axon in the TrkB-Fc group.

Statistical analysis

Aligned rank transform for non-parametric factorial 2-way mixed design model with BDNF manipulation as between-subject and visual stimulation (**Figures 1E-F and 2E-F**) or time (**Figures 3E-G and 4D**) as within-subject factor was performed using ART tool package implemented in R (Wobbrock et al., 2011). After obtaining significant interaction, to

assess statistical significance of simple main effects, either Kruskal-Wallis or Friedman's test, followed by pairwise post-hoc tests corrected for multiple comparisons using the Benjamini, Krieger and Yekutieli (BKY) two-stage linear step-up procedure (Benjamini et al., 2006) were carried out using GraphPad Prism 9.0.0 and the results of the tests used for each experiment are described for each figure legend and in supplemental table 1. The axonal reconstructions and their spanning fields in **Figure 4A-C** were plotted using Plotly.

Figure legends

Figure 1. Blocking distinct components of BDNF signaling differentially affects correlation-dependent branch dynamics

(A) Retinal co-electroporation of EGFP and MO to label ipsi axons with receptor knock-down. Two-photon z-series projection of ipsi axon with EGFP (cyan) and lissamine-tagged Ctrl-MO (magenta). For TrkB-Fc experiments, intraventricular injection was performed >1 h prior to imaging. (B) Visual stimulation (10 ms light flash; 0.5 Hz) delivered via optic fibers positioned by the tadpoles' eyes. Ipsi axons were imaged every 10 min: 1 h Darkness, 1.5 h or 2 h Asynchronous, 1.5 h or 2h Synchronous stimulation (DAS: shorter protocol used for intraventricular TrkB-Fc) (C) Reconstructed arbors showing added, lost and transient branches. Drawings summarize branch dynamics over 1 h. Timecourse of branch (D) additions and (E) losses normalized to the average in darkness, DAS (1 h, 1.5 h, 1.5 h). Average branch (F) addition and (G) loss rates per first hour of stimulation. Significant interactions in the two-way mixed design model: (F) $p = 0.02347$; (G) $p = 0.00149$. (within-subject factor: stimulation; between-subject factor: BDNF manipulation); Post-hoc tests corrected for multiple comparisons (BKY two-stage linear step-up procedure): $^{*}p \leq 0.05$, $^{**}p \leq 0.01$. Graphs show (D-E) mean ± s.e.m. and (F-G) median and individual data points. Scale bars: (A) 20 µm; (B) 500 µm.

Figure 2. Role of BDNF signaling in local axonal branch elimination induced by synchronous stimulation.

(A) Three consecutive reconstructed arbors from a control ipsi axon during synchronous stimulation. Addition and elimination events (for timepoint "*t*") are defined as the coordinates of the branch point of the newly added axonal branch (≥ 1.5 µm) between *t-10 min* and *t* (blue), or terminal point of a lost branch between *t* and *t+10 min* (magenta), respectively. (B) All elimination events during DAS (1 h, 1.5 h, 1.5 h) are superimposed on the reconstructed arbor (last timepoint of each stimulation period). (C) Illustration of distances between an elimination event and all the other events (pair distances). (D) All the elimination event pair distances for the axon from (B). Means are denoted as yellow crosses. Normalized branch (E) elimination and (F) addition event pair distances. To correct for changes in arbor size, each point represents the ratio of observed-to-

randomized (**Figure S2**) mean event pair distances, normalized to darkness for each axon. Significant interaction in the two-way mixed design model: (E) $p<0.001$; Post-hoc tests corrected for multiple comparisons (BKY two-stage linear step-up procedure): *$p \leq 0.05$, ‡$p \leq 0.05$ compared to control. Bars represent median.

Figure 3. Effects of retinal TrkB-MO and p75-MO on RGC axonal arbor elaboration over days

(A-C) Two-photon Z-series projections over 4 d for example axons co-electroporated with EGFP and (A) Ctrl-MO, (B) p75-MO, (C) TrkB-MO. (D) Reconstructed control arbor from day *4* showing axonal skeleton (black), terminal segments (blue) and terminal points (orange). (E-F) Morphometric analysis including (E) number of terminal points and (F) skeleton length, normalized to day 1. (G) Distribution of terminal segments (percent of total per axon) binned by length. Significant interactions in the two-way mixed design model: (E-F) $p <0.001$; (G) $p = 0.04394$ (<5 μm bin); $p = 0.01981$ (5-10 μm bin). Post-hoc tests corrected for multiple comparisons (BKY two-stage linear step-up procedure): (E-F) *$p \leq 0.05$, **$p \leq 0.01$ and (G) comparison between day 1 and day 4, (G) comparison between day 2 and day 4: #$p \leq 0.05$, ##$p \leq 0.01$, ###$p \leq 0.001$, (G) comparison between day 3 and day 4: ‡$p \leq 0.05$, ‡‡$p \leq 0.01$. Data represent (E-F) median and individual data points, and (G) median ± iqr. Scale bar: 20 μm applies to all images.

Figure 4. Opposing effects of retinal TrkB-MO and p75-MO on RGC axon arbor span compactness

(A-C) Three-dimensional spans of reconstructed RGC axon arbors over 4 days, co-electroporated with EGFP and MO: (A) Ctrl-MO, (B) p75-MO, and (C) TrkB-MO. (D) Significant interaction in the two-way mixed design model: **$p =0.00119$. (E) TrkB-MO leads to a faster increase in arbor spanning field volume compared to p75-MO [Arbor spanning field expansion index = (day 4 - day 1)/(day 1 + day 4)], analyzed by Kruskal-Wallis test, $p = 0.0175$ and pairwise post-hoc tests corrected for multiple comparisons: **$p \leq 0.01$. Data represent (D) median and individual points, and (E) median ± iqr. (F) Summary schematic of structural remodeling of an RGC axon instructed by patterned activity: correlated firing (left) and non-correlated firing (right) of axon with neighboring

inputs and postsynaptic partner. Zoom-in of proposed molecular and cellular mechanisms underlying (G) Stentian and (H) Hebbian structural plasticity in the developing visual system.

Supplemental figures

Figure S1, related to Figure 1: Validation of p75-MO and TrkB-MO

(A) Schematic of the mRNA constructs encoding $p75^{NTR}$-EGFP fusion protein. Binding of p75-MO to the *$p75^{NTR}$*-5'UTR-containing mRNA (p75-EGFP mRNA; left) impedes mRNA translation, whereas the inability of p75-MO to bind the construct lacking the *$p75^{NTR}$* 5'UTR (MO-resistant p75-EGFP mRNA; right) spares mRNA translation. (B) Schematic of mRNA construct and MO injection at 2-cell stage, raising injected embryos to stage 26 and preparation of whole-animal homogenates. (C) Western blot analysis of homogenates derived from animals injected with combination of p75-EGFP mRNA or MO-resistant p75-EGFP mRNA and p75-MO probed for EGFP and β-tubulin. (D) Schematic of MO injection at 2-cell stage, followed by intraventricular injection of BDNF in morphant tadpoles at stage 46, 1 h before brain homogenate preparation. (E) Western blot analysis of brain homogenates probed for phospho-Trk (p-Trk) and β-tubulin. Approximate size (kDa) is shown next to the bands

Figure S2, related to Figure 2: Monte Carlo simulation of addition and elimination event pair distances

Mean simulated (A) elimination and (B) addition event pair distances in DAS (1 h, 1.5 h, 1.5 h) by redistribution of events at random within the reconstructed arbor. Data represent median and individual data points. Significant interaction in the two-way mixed design model: (A) $p = 0.0024611$; (B) $p<0.001$. Pairwise post-hoc tests corrected for multiple comparisons (BKY two-stage linear step-up procedure): *$p \leq 0.05$, **$p \leq 0.01$, ‡$p \leq 0.05$, compared to control.

References

Alsina, B., Vu, T., and Cohen-Cory, S. (2001). Visualizing synapse formation in arborizing optic axons in vivo: dynamics and modulation by BDNF. Nat. Neurosci. *4*, 1093–1101.

Baho, E., Chattopadhyaya, B., Lavertu-Jolin, M., Mazziotti, R., Awad, P.N., Chehrazi, P., Groleau, M., Jahannault-Talignani, C., Vaucher, E., Ango, F., et al. (2019). p75 Neurotrophin Receptor Activation Regulates the Timing of the Maturation of Cortical Parvalbumin Interneuron Connectivity and Promotes Juvenile-like Plasticity in Adult Visual Cortex. J. Neurosci. *39*, 4489–4510.

Balkowiec, A., and Katz, D.M. (2000). Activity-Dependent Release of Endogenous Brain-Derived Neurotrophic Factor from Primary Sensory Neurons Detected by ELISAIn Situ. J. Neurosci. *20*, 7417–7423.

Benjamini, Y., Krieger, A.M., and Yekutieli, D. (2006). Adaptive linear step-up procedures that control the false discovery rate. Biometrika *93*, 491–507.

Bird, A.D., and Cuntz, H. (2019). Dissecting Sholl Analysis into Its Functional Components. Cell Rep. *27*, 3081-3096.e5.

Bronfman, F.C., and Fainzilber, M. (2004). Multi-tasking by the p75 neurotrophin receptor: sortilin things out? EMBO Rep. *5*, 867–871.

Chao, M.V., and Hempstead, B.L. (1995). p75 and Trk: a two-receptor system. Trends Neurosci. *18*, 321–326.

Cline, H., and Haas, K. (2008). The regulation of dendritic arbor development and plasticity by glutamatergic synaptic input: a review of the synaptotrophic hypothesis. J. Physiol. *586*, 1509–1517.

Cline, H.T., Debski, E.A., and Constantine-Paton, M. (1987). N-methyl-D-aspartate receptor antagonist desegregates eye-specific stripes. Proc. Natl. Acad. Sci. U. S. A. *84*, 4342–4345.

Cohen-Cory, S., and Fraser, S.E. (1995). Effects of brain-derived neurotrophic factor on optic axon branching and remodelling in vivo. Nature *378*, 192–196.

Coupé, P., Munz, M., Manjón, J.V., Ruthazer, E.S., and Collins, D.L. (2012). A CANDLE for a deeper in vivo insight. Med. Image Anal. *16*, 849–864.

Cuntz, H., Forstner, F., Borst, A., and Häusser, M. (2010). One rule to grow them all: a general theory of neuronal branching and its practical application. PLoS Comput. Biol. *6*.

Demas, J.A., Payne, H., and Cline, H.T. (2012). Vision drives correlated activity without patterned spontaneous activity in developing Xenopus retina. Dev. Neurobiol. *72*, 537–

546.

Dhande, O.S., Hua, E.W., Guh, E., Yeh, J., Bhatt, S., Zhang, Y., Ruthazer, E.S., Feller, M.B., and Crair, M.C. (2011). Development of single retinofugal axon arbors in normal and β2 knock-out mice. J. Neurosci. *31*, 3384–3399.

Dieni, S., Matsumoto, T., Dekkers, M., Rauskolb, S., Ionescu, M.S., Deogracias, R., Gundelfinger, E.D., Kojima, M., Nestel, S., Frotscher, M., et al. (2012). BDNF and its pro-peptide are stored in presynaptic dense core vesicles in brain neurons. J. Cell Biol. *196*, 775–788.

Dougherty, K.D., and Milner, T.A. (1999). p75NTR immunoreactivity in the rat dentate gyrus is mostly within presynaptic profiles but is also found in some astrocytic and postsynaptic profiles. J. Comp. Neurol. *407*, 77–91.

Du, J.-L., and Poo, M.-M. (2004). Rapid BDNF-induced retrograde synaptic modification in a developing retinotectal system. Nature *429*, 878–883.

Dziembowska, M., Milek, J., Janusz, A., Rejmak, E., Romanowska, E., Gorkiewicz, T., Tiron, A., Bramham, C.R., and Kaczmarek, L. (2012). Activity-dependent local translation of matrix metalloproteinase-9. J. Neurosci. *32*, 14538–14547.

Gore, S.V., James, E.J., Huang, L.-C., Park, J.J., Berghella, A., Thompson, A., Cline, H.T., and Aizenman, C. (2021). Role of matrix metalloproteinase-9 in neurodevelopmental disorders and plasticity in Xenopus tadpoles. Elife *10*, e62147.

Guo, W., Nagappan, G., and Lu, B. (2018). Differential effects of transient and sustained activation of BDNF-TrkB signaling. Dev. Neurobiol. *78*, 647–659.

Haapasalo, A., Sipola, I., Larsson, K., Åkerman, K.E.O., Stoilov, P., Stamm, S., Wong, G., and Castrén, E. (2002). Regulation of TRKB Surface Expression by Brain-derived Neurotrophic Factor and Truncated TRKB Isoforms*. J. Biol. Chem. *277*, 43160–43167.

Haas, K., Li, J., and Cline, H.T. (2006). AMPA receptors regulate experience-dependent dendritic arbor growth in vivo. Proc. Natl. Acad. Sci. U. S. A. *103*, 12127–12131.

Harward, S.C., Hedrick, N.G., Hall, C.E., Parra-Bueno, P., Milner, T.A., Pan, E., Laviv, T., Hempstead, B.L., Yasuda, R., and McNamara, J.O. (2016). Autocrine BDNF-TrkB signalling within a single dendritic spine. Nature *538*, 99–103.

Hebb, D.O. (1949). The Organization of Behavior:A Neuropsychological Theory (New York: John Wiley).

Hermey, G., Riedel, I.B., Rezgaoui, M., Westergaard, U.B., Schaller, C., and Hermans-Borgmeyer, I. (2001). SorCS1, a member of the novel sorting receptor family, is localized in somata and dendrites of neurons throughout the murine brain. Neurosci. Lett. *313*, 83–87.

Holt, C.E., and Harris, W.A. (1983). Order in the initial retinotectal map in Xenopus: a new technique for labelling growing nerve fibres. Nature *301*, 150–152.

Horch, H.W., and Katz, L.C. (2002). BDNF release from single cells elicits local dendritic growth in nearby neurons. Nat. Neurosci. *5*, 1177–1184.

Hu, B., Nikolakopoulou, A.M., and Cohen-Cory, S. (2005). BDNF stabilizes synapses and maintains the structural complexity of optic axons in vivo. Development *132*, 4285–4298.

Je, H.S., Yang, F., Ji, Y., Nagappan, G., Hempstead, B.L., and Lu, B. (2012). Role of pro-brain-derived neurotrophic factor (proBDNF) to mature BDNF conversion in activity-dependent competition at developing neuromuscular synapses. Proc. Natl. Acad. Sci. U. S. A. *109*, 15924–15929.

Je, H.S., Yang, F., Ji, Y., Potluri, S., Fu, X.-Q., Luo, Z.-G., Nagappan, G., Chan, J.P., Hempstead, B., Son, Y.-J., et al. (2013). ProBDNF and mature BDNF as punishment and reward signals for synapse elimination at mouse neuromuscular junctions. J. Neurosci. *33*, 9957–9962.

Ji, Y., Lu, Y., Yang, F., Shen, W., Tang, T.T.-T., Feng, L., Duan, S., and Lu, B. (2010). Acute and gradual increases in BDNF concentration elicit distinct signaling and functions in neurons. Nat. Neurosci. *13*, 302–309.

Kesner, P., Schohl, A., Warren, E.C., Ma, F., and Ruthazer, E.S. (2020). Postsynaptic and Presynaptic NMDARs Have Distinct Roles in Visual Circuit Development. Cell Rep. *32*, 107955.

Kirchner, J.H., and Gjorgjieva, J. (2021). Emergence of local and global synaptic organization on cortical dendrites. Nat. Commun. *12*, 1–18.

Kohara, K., Yasuda, H., Huang, Y., Adachi, N., Sohya, K., and Tsumoto, T. (2007). A local reduction in cortical GABAergic synapses after a loss of endogenous brain-derived neurotrophic factor, as revealed by single-cell gene knock-out method. J. Neurosci. *27*, 7234–7244.

Kutsarova, E., Munz, M., and Ruthazer, E.S. (2016). Rules for Shaping Neural Connections in the Developing Brain. Front. Neural Circuits *10*, 111.

López-Bendito, G., and Molnár, Z. (2003). Thalamocortical development: how are we going to get there? Nat. Rev. Neurosci. *4*, 276–289.

Marshak, S., Nikolakopoulou, A.M., Dirks, R., Martens, G.J., and Cohen-Cory, S. (2007). Cell-autonomous TrkB signaling in presynaptic retinal ganglion cells mediates axon arbor growth and synapse maturation during the establishment of retinotectal synaptic connectivity. J. Neurosci. *27*, 2444–2456.

McLaughlin, T., Hindges, R., and O'Leary, D.D.M. (2003). Regulation of axial patterning

of the retina and its topographic mapping in the brain. Curr. Opin. Neurobiol. *13*, 57–69.

Meyer, M.P., and Smith, S.J. (2006). Evidence from in vivo imaging that synaptogenesis guides the growth and branching of axonal arbors by two distinct mechanisms. J. Neurosci. *26*, 3604–3614.

Mowla, S.J., Pareek, S., Farhadi, H.F., Petrecca, K., Fawcett, J.P., Seidah, N.G., Morris, S.J., Sossin, W.S., and Murphy, R.A. (1999). Differential sorting of nerve growth factor and brain-derived neurotrophic factor in hippocampal neurons. J. Neurosci. *19*, 2069–2080.

Mrsic-Flogel, T.D., Hofer, S.B., Creutzfeldt, C., Cloëz-Tayarani, I., Changeux, J.-P., Bonhoeffer, T., and Hübener, M. (2005). Altered map of visual space in the superior colliculus of mice lacking early retinal waves. J. Neurosci. *25*, 6921–6928.

Mu, Y., and Poo, M.-M. (2006). Spike timing-dependent LTP/LTD mediates visual experience-dependent plasticity in a developing retinotectal system. Neuron *50*, 115–125.

Munz, M., Gobert, D., Schohl, A., Poquérusse, J., Podgorski, K., Spratt, P., and Ruthazer, E.S. (2014). Rapid Hebbian axonal remodeling mediated by visual stimulation. Science *344*, 904–909.

Niculescu, D., Michaelsen-Preusse, K., Güner, Ü., van Dorland, R., Wierenga, C.J., and Lohmann, C. (2018). A BDNF-Mediated Push-Pull Plasticity Mechanism for Synaptic Clustering. Cell Rep. *24*, 2063–2074.

Nieuwkoop, P.D., and Faber J.(1994). Normal table of Xenopus laevis (Daudin): a systematical and chronological survey of the development from the fertilized egg till the end of metamorphosis (New York: Garland Pub.)

Ohba, S., Ikeda, T., Ikegaya, Y., Nishiyama, N., Matsuki, N., and Yamada, M.K. (2005). BDNF locally potentiates GABAergic presynaptic machineries: target-selective circuit inhibition. Cereb. Cortex *15*, 291–298.

Orefice, L.L., Shih, C.-C., Xu, H., Waterhouse, E.G., and Xu, B. (2016). Control of spine maturation and pruning through proBDNF synthesized and released in dendrites. Mol. Cell. Neurosci. *71*, 66–79.

Pang, P.T., Teng, H.K., Zaitsev, E., Woo, N.T., Sakata, K., Zhen, S., Teng, K.K., Yung, W.-H., Hempstead, B.L., and Lu, B. (2004). Cleavage of proBDNF by tPA/plasmin is essential for long-term hippocampal plasticity. Science *306*, 487–491.

Qian, Z., Gilbert, M.E., Colicos, M.A., Kandel, E.R., and Kuhl, D. (1993). Tissue-plasminogen activator is induced as an immediate-early gene during seizure, kindling and long-term potentiation. Nature *361*, 453–457.

Rahman, T.N., Munz, M., Kutsarova, E., Bilash, O.M., and Ruthazer, E.S. (2020).

Stentian structural plasticity in the developing visual system. Proc. Natl. Acad. Sci. U. S. A. *117*, 10636–10638.

Rajan, I., Witte, S., and Cline, H.T. (1999). NMDA receptor activity stabilizes presynaptic retinotectal axons and postsynaptic optic tectal cell dendrites in vivo. J. Neurobiol. *38*, 357–368.

Rösch, H., Schweigreiter, R., Bonhoeffer, T., Barde, Y.-A., and Korte, M. (2005). The neurotrophin receptor p75NTR modulates long-term depression and regulates the expression of AMPA receptor subunits in the hippocampus. Proc. Natl. Acad. Sci. U. S. A. *102*, 7362–7367.

Rossi, F.M., Pizzorusso, T., Porciatti, V., Marubio, L.M., Maffei, L., and Changeux, J.P. (2001). Requirement of the nicotinic acetylcholine receptor beta 2 subunit for the anatomical and functional development of the visual system. Proc. Natl. Acad. Sci. U. S. A. *98*, 6453–6458.

Ruthazer, E.S., Akerman, C.J., and Cline, H.T. (2003). Control of axon branch dynamics by correlated activity in vivo. Science *301*, 66–70.

Ruthazer, E.S., Li, J., and Cline, H.T. (2006). Stabilization of axon branch dynamics by synaptic maturation. J. Neurosci. *26*, 3594–3603.

Schindelin, J. *et al.* (2012) “Fiji: an open-source platform for biological-image analysis,” *Nature methods*, 9(7), pp. 676–682.

Schwartz, N., Schohl, A., and Ruthazer, E.S. (2011). Activity-dependent transcription of BDNF enhances visual acuity during development. Neuron *70*, 455–467.

Smear, M.C., Tao, H.W., Staub, W., Orger, M.B., Gosse, N.J., Liu, Y., Takahashi, K., Poo, M.-M., and Baier, H. (2007). Vesicular glutamate transport at a central synapse limits the acuity of visual perception in zebrafish. Neuron *53*, 65–77.

Stent, G.S. (1973). A physiological mechanism for Hebb’s postulate of learning. Proc. Natl. Acad. Sci. U. S. A. *70*, 997–1001.

Strahler, A.N. (1957). Quantitative analysis of watershed geomorphology. Trans. Engl. Ceram. Circle *38*, 913.

Uylings, H.B., Smit, G.J., and Veltman, W.A. (1975). Ordering methods in quantitative analysis of branching structures of dendritic trees. Adv. Neurol. *12*, 347–354.

Vignoli, B., Battistini, G., Melani, R., Blum, R., Santi, S., Berardi, N., and Canossa, M. (2016). Peri-Synaptic Glia Recycles Brain-Derived Neurotrophic Factor for LTP Stabilization and Memory Retention. Neuron *92*, 873–887.

Vormberg, A., Effenberger, F., Muellerleile, J., and Cuntz, H. (2017). Universal features of dendrites through centripetal branch ordering. PLoS Comput. Biol. *13*, e1005615.

Wang, X., Chun, S.-J., Treloar, H., Vartanian, T., Greer, C.A., and Strittmatter, S.M. (2002). Localization of Nogo-A and Nogo-66 receptor proteins at sites of axon-myelin and synaptic contact. J. Neurosci. *22*, 5505–5515.

Winnubst, J., Cheyne, J.E., Niculescu, D., and Lohmann, C. (2015). Spontaneous Activity Drives Local Synaptic Plasticity In Vivo. Neuron *87*, 399–410.

Wobbrock, J.O., Findlater, L., Gergle, D., and Higgins, J.J. (2011). The aligned rank transform for nonparametric factorial analyses using only anova procedures. In Proceedings of the SIGCHI Conference on Human Factors in Computing Systems, (New York, NY, USA: Association for Computing Machinery), pp. 143–146.

Woo, N.H., Teng, H.K., Siao, C.-J., Chiaruttini, C., Pang, P.T., Milner, T.A., Hempstead, B.L., and Lu, B. (2005). Activation of p75NTR by proBDNF facilitates hippocampal long-term depression. Nat. Neurosci. *8*, 1069–1077.

Yang, J., Siao, C.-J., Nagappan, G., Marinic, T., Jing, D., McGrath, K., Chen, Z.-Y., Mark, W., Tessarollo, L., Lee, F.S., et al. (2009). Neuronal release of proBDNF. Nat. Neurosci. *12*, 113–115.

Yang, J., Harte-Hargrove, L.C., Siao, C.-J., Marinic, T., Clarke, R., Ma, Q., Jing, D., Lafrancois, J.J., Bath, K.G., Mark, W., et al. (2014). proBDNF negatively regulates neuronal remodeling, synaptic transmission, and synaptic plasticity in hippocampus. Cell Rep. *7*, 796–806.

Zagrebelsky, M., and Korte, M. (2014). Form follows function: BDNF and its involvement in sculpting the function and structure of synapses. Neuropharmacology *76 Pt C*, 628–638.

Zhang, X.H., and Poo, M.-M. (2002). Localized synaptic potentiation by BDNF requires local protein synthesis in the developing axon. Neuron *36*, 675–688.

Zhang, J., Ackman, J.B., Xu, H.-P., and Crair, M.C. (2011). Visual map development depends on the temporal pattern of binocular activity in mice. Nat. Neurosci. *15*, 298–307.

Zou, D.J., and Cline, H.T. (1996). Expression of constitutively active CaMKII in target tissue modifies presynaptic axon arbor growth. Neuron *16*, 529–539.

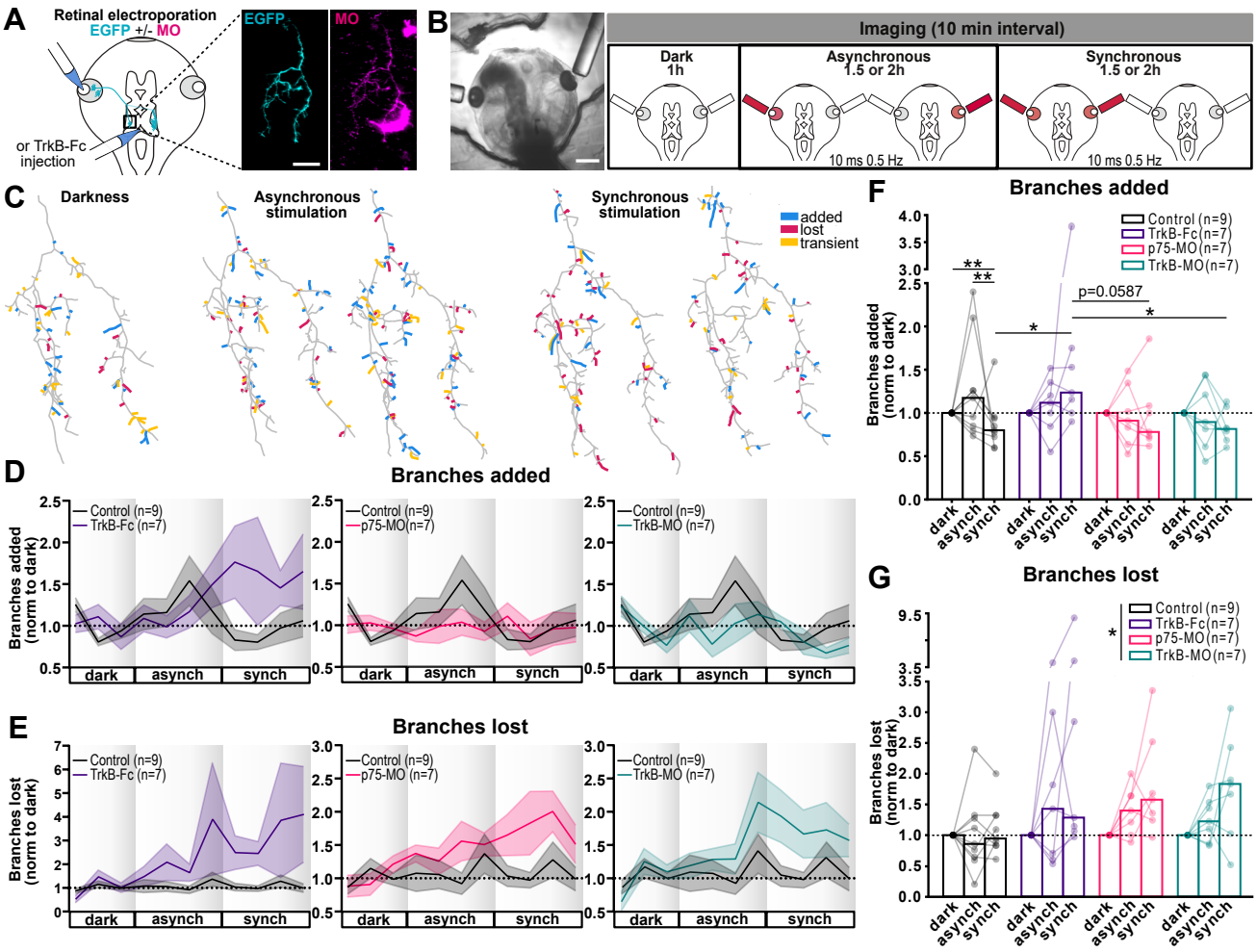
A
Retinal electroporation
EGFP +/- MO
or TrkB-Fc injection
EGFP
MO
B
Imaging (10 min interval)
Dark 1h
Asynchronous 1.5 or 2h
Synchronous 1.5 or 2h
10 ms 0.5 Hz
10 ms 0.5 Hz
C
Darkness
Asynchronous stimulation
Synchronous stimulation
added
lost
transient
D
Branches added
Branches added (norm to dark)
Control (n=9)
TrkB-Fc (n=7)
p75-MO(n=7)
TrkB-MO (n=7)
dark
asynch
synch
E
Branches lost
Branches lost (norm to dark)
F
Branches added
Control (n=9)
TrkB-Fc(n=7)
p75-MO(n=7)
TrkB-MO(n=7)
p=0.0587
G
Branches lost

Figure 1

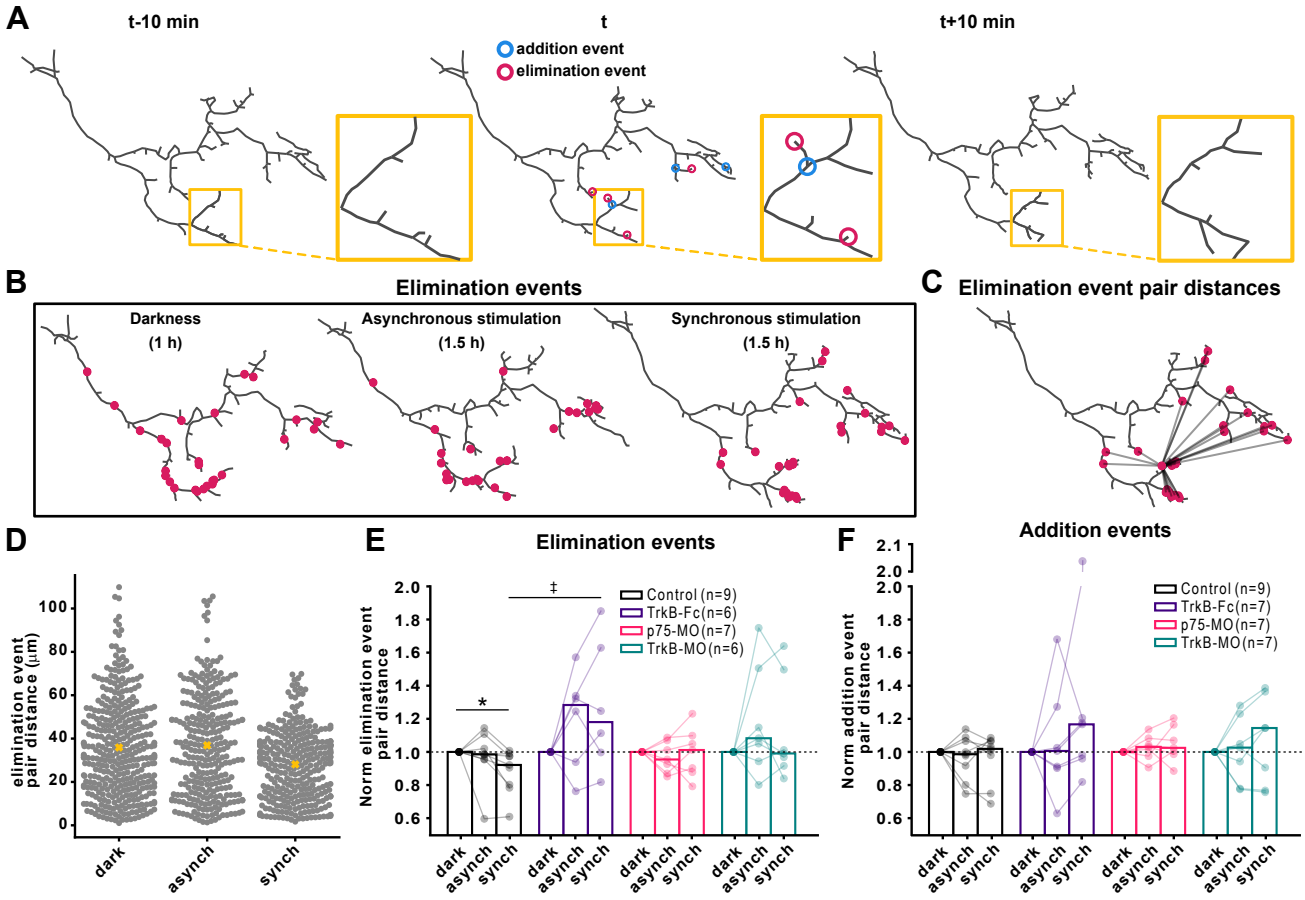
A
t-10 min
t
addition event
elimination event
t+10 min
B
Elimination events
Darkness
(1 h)
Asynchronous stimulation
(1.5 h)
Synchronous stimulation
(1.5 h)
C
Elimination event pair distances
D
elimination event pair distance (µm)
dark
asynch
synch
E
Elimination events
Norm elimination event pair distance
Control (n=9)
TrkB-Fc(n=6)
p75-MO(n=7)
TrkB-MO(n=6)
F
Addition events
Norm addition event pair distance
Control (n=9)
TrkB-Fc(n=7)
p75-MO(n=7)
TrkB-MO(n=7)

Figure 2

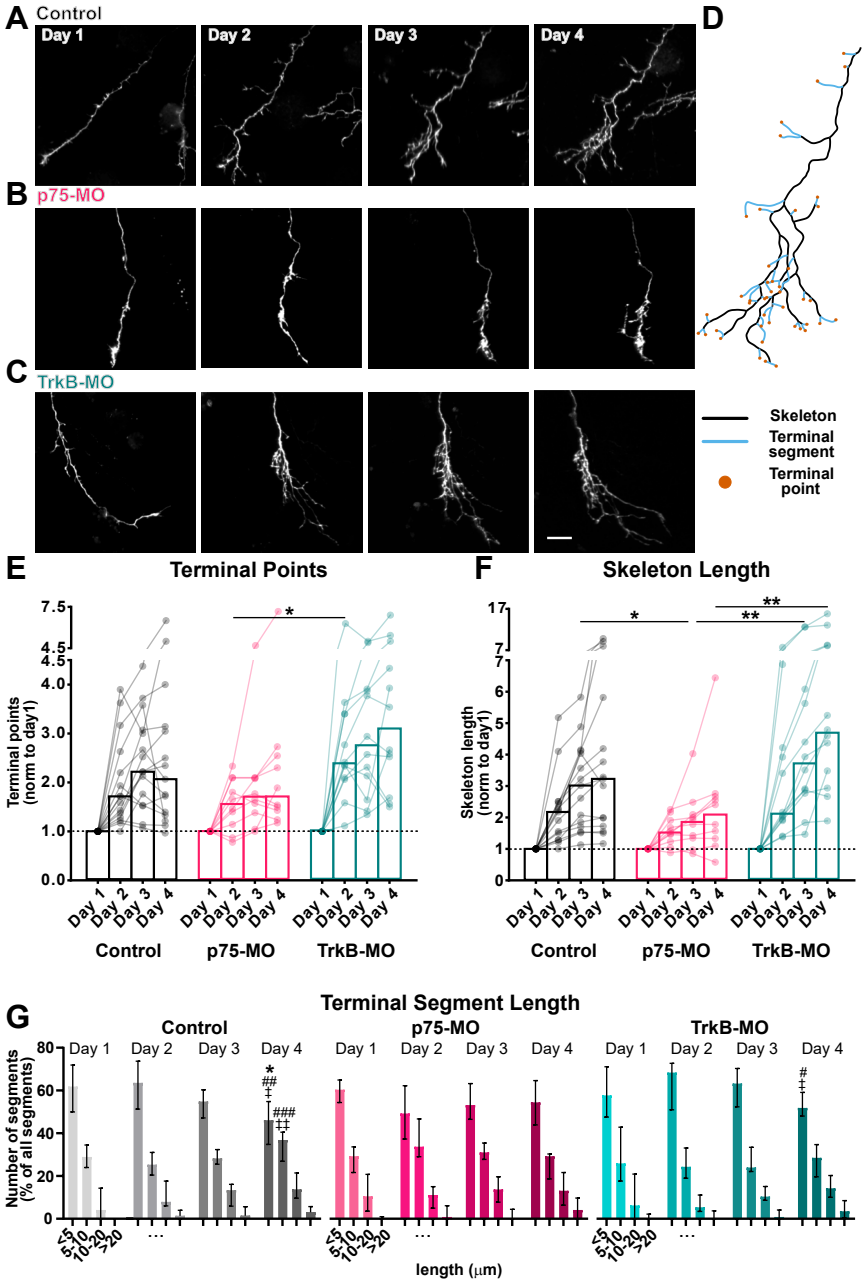
A
Control
Day 1
Day 2
Day 3
Day 4
B
p75-MO
C
TrkB-MO
D
Skeleton
Terminal segment
Terminal point
E
Terminal Points
Terminal points (norm to day1)
Control
p75-MO
TrkB-MO
F
Skeleton Length
Skeleton length (norm to day1)
G
Terminal Segment Length
Number of segments (% of all segments)
length (μm)

Figure 3

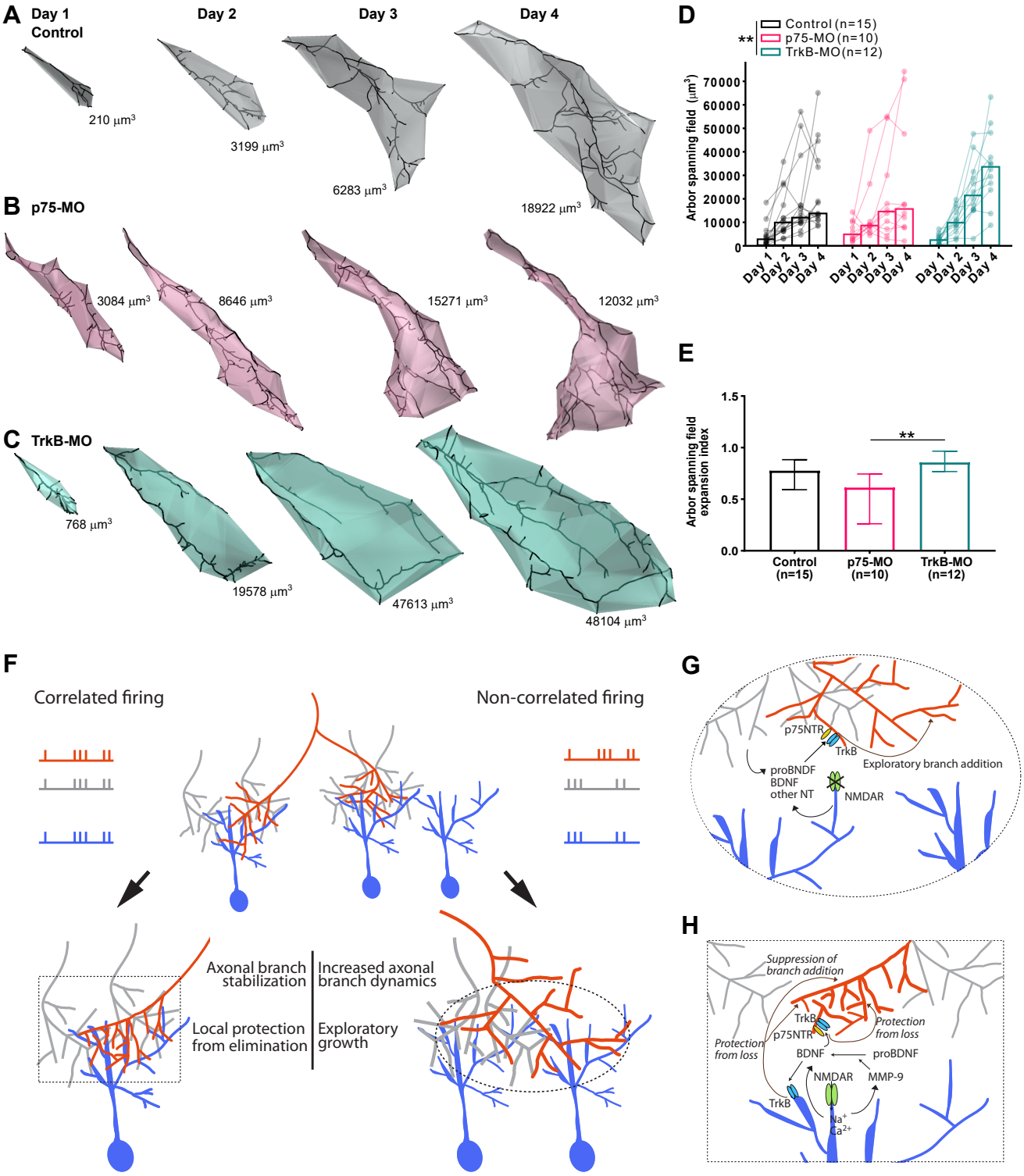
A
Day 1
Control
Day 2
Day 3
Day 4
210 μm³
3199 μm³
6283 μm³
18922 μm³
B
p75-MO
3084 μm³
8646 μm³
15271 μm³
12032 μm³
C
TrkB-MO
768 μm³
19578 μm³
47613 μm³
48104 μm³
D
Control (n=15)
p75-MO (n=10)
TrkB-MO (n=12)
**
Arbor spanning field (μm³)
70000
60000
50000
40000
30000
20000
10000
0
Day 1
Day 2
Day 3
Day 4
E
Arbor spanning field expansion index
1.5
1.0
0.5
0.0
**
Control (n=15)
p75-MO (n=10)
TrkB-MO (n=12)
F
Correlated firing
Non-correlated firing
Axonal branch stabilization
Increased axonal branch dynamics
Local protection from elimination
Exploratory growth
G
p75NTR
TrkB
Exploratory branch addition
proBNDF
BDNF
other NT
NMDAR
H
Suppression of branch addition
TrkB
p75NTR
Protection from loss
Protection from loss
BDNF
proBDNF
NMDAR
MMP-9
TrkB
Na+
Ca2+

Figure 4